Supplementary Material to Mas e Braga et al., "Sensitivity of the Antarctic ice sheets to the peak warming of Marine Isotope Stage 11"

Calibration of the ice shelf basal melting parameterisation

As described in Sect. 2.1 (main text), melting rates at the base of ice shelves are computed through a parameterisation based on Beckmann and Goosse (2003), following the form presented in Martin et al. (2011), but with a quadratic dependence on thermal forcing (Holland et al., 2008):

$$Q_{\mathrm{bm}} = F_{\mathrm{melt}} \cdot \frac{\rho_{\mathrm{sw}} c_{\mathrm{p_0}} \gamma_T T_{\mathrm{force}} |T_{\mathrm{force}}|}{L_{\mathrm{i}} \rho_{\mathrm{i}}} \tag{1}$$

where $c_{\mathrm{p_0}}$ is the specific heat capacity of the ocean mixed layer (3974 J kg^{-1} K^{-1}), γ_{T} the thermal change velocity (10^{-4} m s^{-1}), ρ_{ice} is the density of ice (910 kg m^{-3}), and L_{i} is the heat capacity (3.35×10^5 J kg^{-1}) of ice. Here, T_{force} is given by

$$T_{\mathrm{force}} = T_{\mathrm{zb}} - T_{\mathrm{melt}} \tag{2}$$

where T_{zb} is the ocean temperature (obtained from the forcing data set) at the depth of the ice shelf base and T_{melt} is calculated from Eq. 2 of Beckmann and Goosse (2003):

$$T_{\mathrm{melt}} = 0.0939 - 0.057 S_{\mathrm{o}} + 7.64 \times 10^{-4} (Z_{\mathrm{b}} - Z_{\mathrm{sl}}) \tag{3}$$

where Z_{b} and Z_{sl} are the modeled depths of the ice shelf base and the sea level respectively, and S_{o} is the average sea water salinity (here a constant value of 35).

We optimize the choice of the melting coefficient F_{melt} by first iteratively adjusting the spatial distribution of basal melting rates, Q_{bm}, over all Antarctic ice shelves (i.e., at every ice shelf grid point) such that it keeps the thickness of each grid point as close as possible to the Bedmap2 data (cf. Bernales et al., 2017). We then derive spatially varying values for F_{melt} through Eq. 5:

$$F_{\mathrm{melt}} = \frac{Q_{\mathrm{bm}} L_{\mathrm{i}} \rho_{\mathrm{i}}}{\rho_{\mathrm{sw}} c_{\mathrm{p_0}} \gamma_T T_{\mathrm{force}} |T_{\mathrm{force}}|} \tag{4}$$

On the one hand, and because model simulations over long time scales need to consider the evolution of ice shelf distribution (including changes in the position of the grounding line), a spatially heterogeneous distribution of F_{melt} is impractical for the experiments presented in this study. On the other hand, the use of a single value for F_{melt} is not able to reproduce the stark difference in magnitude between the melting rates at grounding lines and ice-shelf interiors (cf. Rignot and Jacobs, 2002). We thus redefine the value of F_{melt} as

$$F_{\mathrm{melt}} = (1.0 - W_{\mathrm{fg}})\, F_{\mathrm{melt_{SH}}} + W_{\mathrm{fg}}\, F_{\mathrm{melt_{GL}}} \tag{5}$$

where $F_{melt_{\mathrm{SH}}}$ is a value chosen for ice-shelf interiors (away from the grounding line) and $F_{\mathrm{melt_{GL}}}$ is the value at grounding lines. These two values are weighed by W_{fg}, which varies according to the flux of ice across the grounding line, given by

$$W_{\mathrm{fg}} = \frac{2}{\pi} \tan^{-1} \frac{\Phi_{\mathrm{gl}}^2}{\Phi_{\mathrm{ref}}^2}, \tag{6}$$

where $\Phi_{\text{ref}} = 2 \times 10^5 \text{m}^2\,\text{a}^{-1}$ and Φ_{gl} is the flux across the grounding line also in $\text{m}^2\,\text{a}^{-1}$. The value of Φ_{ref} is simply hand-tuned so that the method identifies the majority of modern flux gates (according to Rignot and Jacobs, 2002; Rignot et al., 2013).

We then find minimum, average, and maximum W_{fg} and $F_{\text{melt}_{\text{GL}}}$ pairs considering only the grid cells where $\Phi_{\text{gl}} > \Phi_{\text{ref}}$ (i.e., what we consider the flux gates). The resulting ideal melting parameter is then obtained by extrapolating the obtained $F_{\text{melt}_{\text{GL}}}$ to what it would be if W_{fg} had a value of 1.0. These values yielded a range between 0.12 and $0.60\,\text{K}^{-1}$. For the ice shelf interior (i.e., $F_{\text{melt}_{\text{SH}}}$), we do a simple averaging of those F_{melt} values obtained that are not located at the grounding line and test values in the range $\overline{F_{\text{melt}_{\text{SH}}}} \pm 4\sigma$, resulting in a range of values from 7.0×10^{-3} to $0.11\,\text{K}^{-1}$, We combine the latter with the range of $F_{\text{melt}_{\text{GL}}}$ values to test for different combinations of these pairs.

All combinations tested yielded 40 steady-state simulations of 10 kyr under CCSM3 PI forcing. We chose the best pair of $F_{\text{melt}_{\text{SH}}}$ and $F_{\text{melt}_{\text{GL}}}$ values based on the run that revealed the least changes compared to the original PI configuration. We find the combination of values that met this criteria to be $0.5\,\text{K}^{-1}$ for $F_{\text{melt}_{\text{GL}}}$ and $8.5 \times 10^{-3}\,\text{K}^{-1}$ for $F_{\text{melt}_{\text{SH}}}$. It is important to stress that the former is very high as it is a hypothetical limit which is never attained due to the weighting applied by W_{fg} during the simulations (see Eq. 6). However, we do identify three regions where the model was not able to sustain a grounding line that matches Present Day (PD) and PI configurations: the southeast part of the Filchner-Ronne Ice Shelf (related to Support Force, Foundation, and Academy ice streams), the Scott Glacier discharge area on the Ross Ice Shelf, and in the strait between George VI Island and the Antarctic Peninsula. The difficulty in accurately representing these sites is not exclusive to our model and has been reported before (e.g., Golledge et al., 2012). Part of this could also be due to inaccuracies in the used topography dataset (Pritchard, 2014; Kingslake et al., 2018). Higher-resolution runs and sub-grid interpolation schemes at the grounding lines could potentially help to solve this problem, but would increase the computational costs of such long runs. These caveats are taken into account when interpreting the results. While this simplification is less realistic than having the melting rate distribution under the entire shelf, it allows to incorporate the calibration into a freely evolving run without having to adjust the basal melting parameters point by point, especially since ice shelf geometries change over a transient simulation. Figure S1a-c shows the resulting PI Surface Mass Balance, the distribution of basal melt rates post-optimization, and the PI topography from which we do the model spinup, respectively.

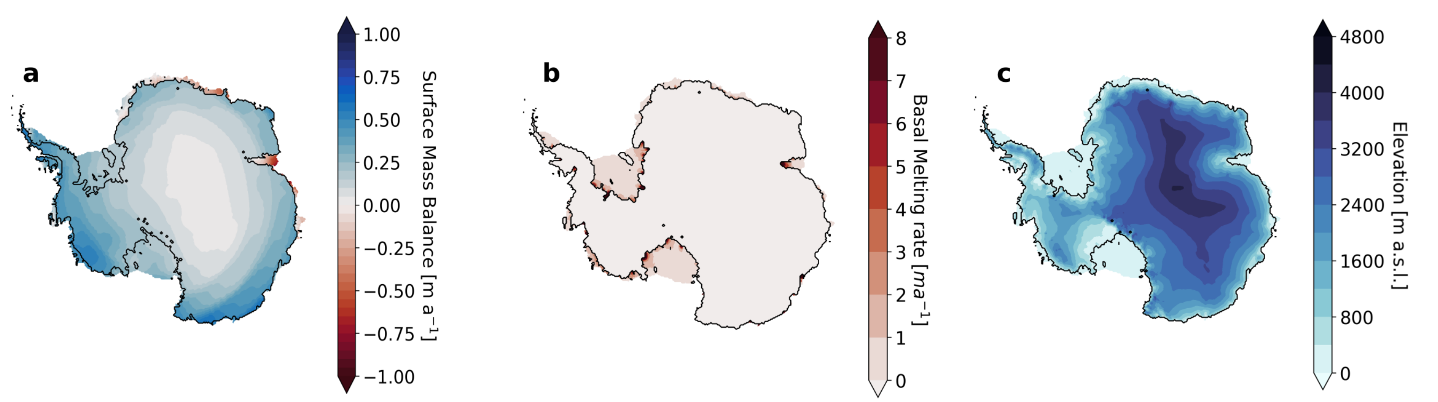

Figure S1: Ice sheet calibration using CCSM3 forcings. (a) Imposed Surface Mass Balance ($\text{m}\,\text{a}^{-1}$) from CCSM3 over the ice sheet during the calibration period. (b) Optimized basal melting rates (Q_{bm} in $\text{m}\,\text{a}^{-1}$) for PI, and (c) resulting PI topography (in meters) and geometry under a steady state from our calibration.

Brief assessment of CCSM3 forcings

The CCSM3 model results used seem to represent surface air temperature satisfactorily given its spatial resolution (T31 spectral resolution), capturing the pattern of colder surfaces in the highest regions in the ice sheet interior, and milder temperatures at its margins and over the Antarctic Peninsula (Figs. S2a,b). Regarding the ocean temperatures, since all datasets for PI or PD of continent-wide sub-shelf ocean temperatures that could be considered as our reference are also highly subject to statistical and model biases, we chose to provide an assessment of the modelled ice-shelf basal melting against observation-inferred values instead (Fig. S2d). As reference we take the calibration procedure that is able to infer the basal melt coefficients under the ice shelves based on the PD topography and atmospheric forcings (c.f. Bernales et al., 2017, Fig. S2c). By comparing the sub ice-shelf basal melt rates (Figs. S2c,d), we can see that the parameterization captures successfully the higher melting rates at the grounding lines of ice streams, but smooths the uneven pattern of melting under more interior regions of the ice shelves, and has little basal melting at the calving front (Figs. S2c,d). One limitation of this method is its inability to represent sub-shelf refreezing. A different parameterization that accounts for this effect has already been developed (Lazeroms et al., 2018), but its implementation for use at paleo timescales has not been done yet. Nevertheless, the absence of this process does not seem to impair our results. As for precipitation (Figs. S2e,f), the model manages to capture the overall pattern, i.e., increased precipitation at the fringes of the ice sheet and less precipitation in the interior. It does not reproduce, however, higher precipitation induced by orography (e.g., west of the Antarctic Peninsula and north of the Transantarctic Mountains), mainly due to the model resolution. Finally, despite the precipitation being significantly lower over the ice sheet interior compared to its margins as expected, the values are significantly overestimated over the interior and underestimated over the high precipitation areas, similar to what has been observed for CMIP5 models (Palerme et al., 2017).

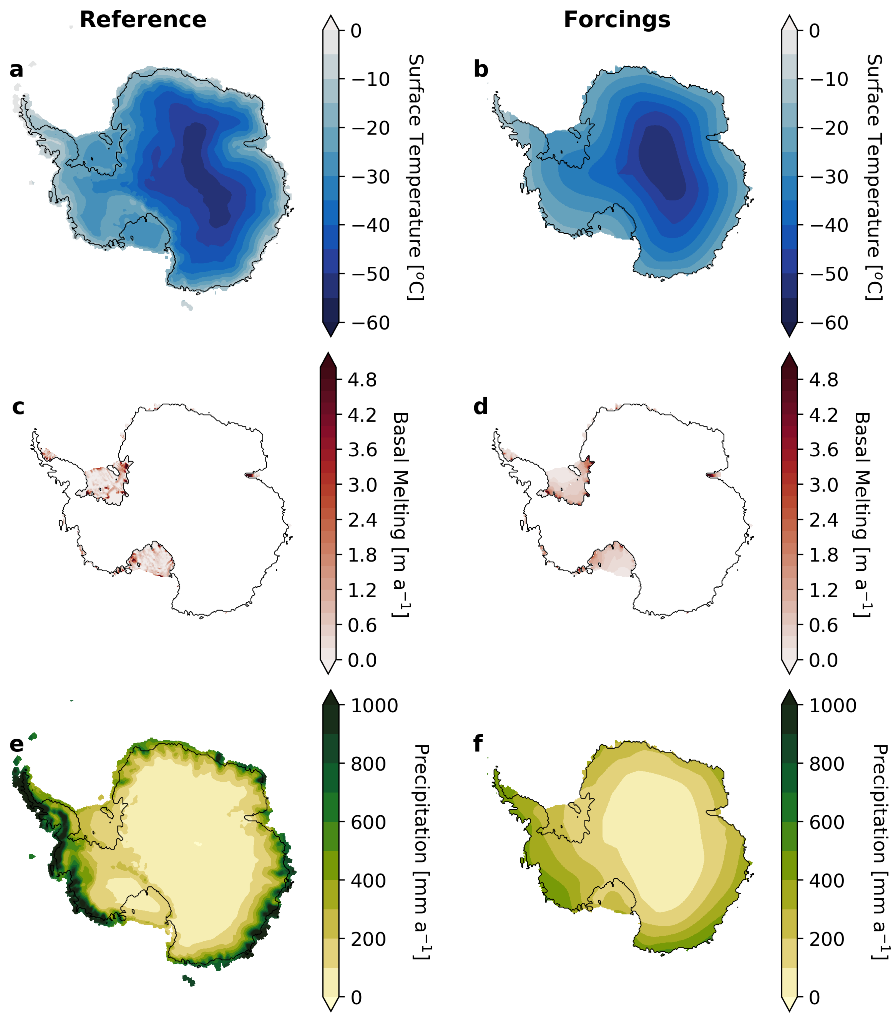

Figure S2: Comparison of CCSM3 forcings (right) to reference data (left) from ERA5 (a,e) and to the calibration of basal melting according to PI forcings (c.f., Bernales et al., 2017). (a,b) surface temperature [°C]; (c,d) basal melting [m a^{-1}]; (e,f) annual precipitation [mm a^{-1}]

Supplementary figures

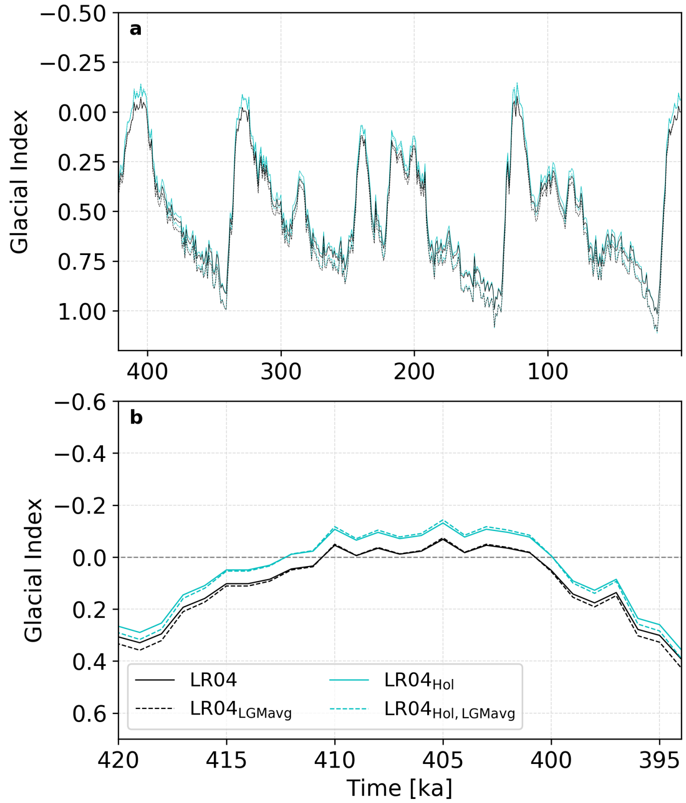

Figure S3: Comparison between the rescaled GI curves for the LR04 stack. "Hol" and "LGMavg" in the legend denote the curves where these different criteria were used in the rescaling, as in the main text (c.f. Fig. 4.

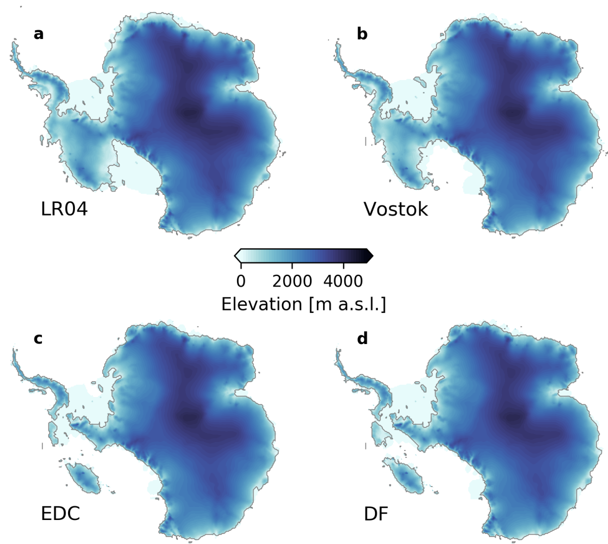

Figure S4: Topography (in m above sea level) of all CFEN members at 405 ka, the time of the global sea-level highstand in our simulations.

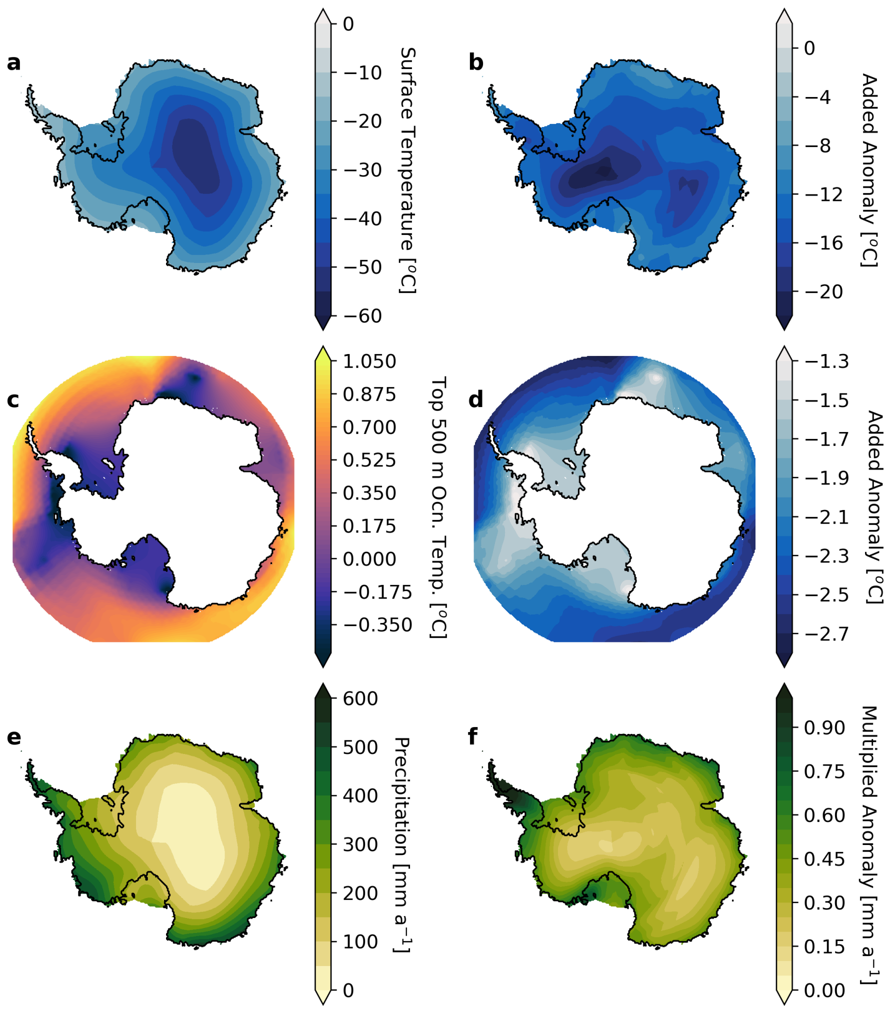

Figure S5: (a-f) Forcing fields used to construct the climate forcings used in this study. Left fields are the PI mean states, while right fields are the anomalies which are multiplied by the GI and then combined with the left-side fields as in Eqs. (2) and (3).

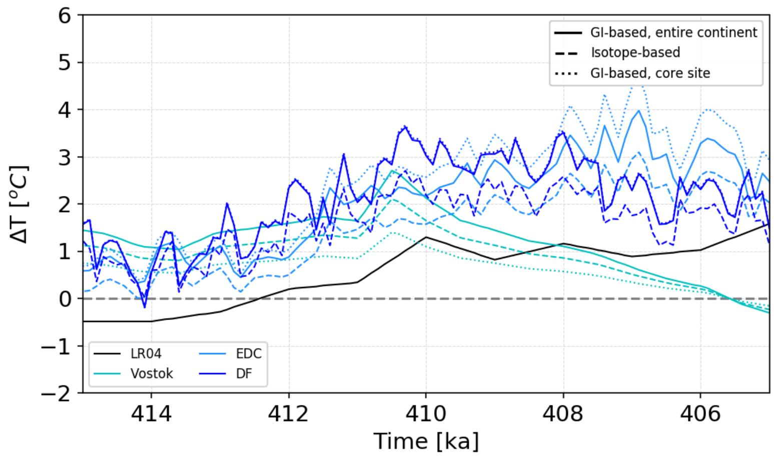

Figure S6: Comparison between the surface atmospheric temperature anomalies obtained by the GI scaling of all ice and sediment cores and the ones reported from the ice cores δD. The GI-scaled temperatures are reported as averages over the entire model domain, while the ones obtained by the scaling of the ice cores are also reported at their respective drilling sites. It is worth mentioning that albeit different, the two DF GI-based temperatures fall very closely to each other, causing a significant overlap.

References

Beckmann, A. and Goosse, H.: A parameterization of ice shelf–ocean interaction for climate models, Ocean modelling, 5, 157–170, 2003.

Bernales, J., Rogozhina, I., and Thomas, M.: Melting and freezing under Antarctic ice shelves from a combination of ice-sheet modelling and observations, Journal of Glaciology, 63, 731–744, 2017.

Golledge, N. R., Fogwill, C. J., Mackintosh, A. N., and Buckley, K. M.: Dynamics of the last glacial maximum Antarctic ice-sheet and its response to ocean forcing, Proceedings of the National Academy of Sciences, 109, 16 052–16 056, 2012.

Holland, P. R., Jenkins, A., and Holland, D. M.: The response of ice shelf basal melting to variations in ocean temperature, Journal of Climate, 21, 2558–2572, 2008.

Kingslake, J., Scherer, R., Albrecht, T., Coenen, J., Powell, R., Reese, R., Stansell, N., Tulaczyk, S., Wearing, M., and Whitehouse, P.: Extensive retreat and re-advance of the West Antarctic Ice Sheet during the Holocene, Nature, 558, 430, 2018.

Lazeroms, W. M. J., Jenkins, A., Gudmundsson, G. H., and Van De Wal, R. S. W.: Modelling present-day basal melt rates for Antarctic ice shelves using a parametrization of buoyant meltwater plumes, The Cryosphere, 12, 49–70, 2018.

Martin, M. A., Winkelmann, R., Haseloff, M., Albrecht, T., Bueler, E., Khroulev, C., and Levermann, A.: The Potsdam Parallel Ice Sheet Model (PISM-PIK)–Part 2: Dynamic equilibrium simulation of the Antarctic Ice Sheet, The Cryosphere, 5, 727–740, 2011.

Palerme, C., Genthon, C., Claud, C., Kay, J. E., Wood, N. B., and L'Ecuyer, T.: Evaluation of current and projected Antarctic precipitation in CMIP5 models, Climate dynamics, 48, 225–239, 2017.

Pritchard, H. D.: Bedgap: where next for Antarctic subglacial mapping?, Antarctic Science, 26, 742–757, 2014.

Rignot, E. and Jacobs, S. S.: Rapid bottom melting widespread near Antarctic Ice Sheet grounding lines, Science, 296, 2020–2023, 2002.

Rignot, E., Jacobs, S., Mouginot, J., and Scheuchl, B.: Ice-shelf melting around Antarctica, Science, 341, 266–270, 2013.